Int. J. Heat Mass Transfer. Vol. 36, No. 10, pp. 2647–2656, 1993
Printed in Great Britain

0017-9310/93 $6.00 + 0.00

Two-dimensional freezing of water filled between vertical concentric tubes involving density anomaly and volume expansion

CHARN-JUNG KIM, SUNG TACK RO,† JOON SIK LEE and MOO GEUN KIM

Department of Mechanical Engineering, Seoul National University, Seoul 151–742, Korea

(*Received* 16 *July* 1992 *and in final form* 8 *October* 1992)

Abstract—Freezing of an initially superheated water filled within an axisymmetric enclosure is studied numerically. Simulation is carried out using a computational method recently developed by the authors to treat moving boundary problems in axisymmetric geometries. Emphasized is the influence of both volume expansion and density anomaly upon freezing via natural convection. Two distinctive types of thermal boundary conditions are identified and utilized to guide our efforts to investigate the freezing process. Due to the density anomaly of pure water, fluid flow direction reverses depending on the initial superheat of water and thereby the interface slope exhibits an inversion behavior. By assuming that the water does not flood over the ice surface, the volume-change-induced rise of ice formed results in a substantially curved surface. Effects of several parameters characterizing phase-change process of interest are investigated. Numerical results clearly reveal that freezing undergoes multiple stages and proceeds in a complicated manner especially when the water is superheated over the density-extremum temperature.

INTRODUCTION

THE INFLUENCE of natural convection on the process of solidification/melting has been extensively studied in recent decades. A comprehensive compilation of researches in this field can be found in refs. [1–3], among others, and hence it is not intended in this study to discuss in detail the current state-of-the-art of the present topic. Generally speaking, it is an accepted fact that natural convection enhances heat transfer rate during melting but retards it during solidification [4].

A survey of literature leads us to recognize that it is a premise to clarify what kinds of thermal boundary conditions are imposed on the liquid phase where natural convection of special interest occurs. For this issue, two essentially distinctive boundary conditions are identified and termed here as *isolated* and *conjugate* types for the sake of concreteness. A conjugate type refers to the case where natural convection in the liquid is everlasting and sustained by a pair of heat source and sink; therefore, quasi-steady assumptions [5–7] can be utilized in determining the flow field owing to the presence of its steady-state solution. Note that in most cases the melting process is of a conjugate type. On the contrary, an isolated type refers to the situation where natural convection eventually fades away. Phase-change problems of isolated type, as frequently encountered in static casting, do not allow for the use of the quasi-steady assumption mentioned above, and thus all the transient terms should be accounted for. In this study, we consider a particular phase-change problem pertaining to an isolated type—freezing of initially superheated water filled between vertical concentric tubes which are subject to convective cooling at the inner tube wall and insulation otherwise. The primary objective is to provide necessary information in designing thermal energy storage systems.

Sparrow *et al.* [4] performed an experimental study of freezing in a cylindrical enclosure. They successfully demonstrated the general characteristics of freezing subject to the thermal boundary conditions of conjugate type. As such, solidification terminated asymptotically in the case of superheated liquid, and this was attributed to the development of natural convection. However, it was pointed out [3] that an equilibrium position of the solid–liquid interface indeed exists even in the absence of natural convection. Ramachandran *et al.* [8] studied solidification in a rectangular enclosure by including the mold effect. Their numerical results showed the decaying of natural convection at larger times, but still not an entire gamut of the multiple stages of solidification. (Solidification undergoing multiple stages is specific to problems of isolated type, as will be elucidated later in this study.) By conducting experiments on freezing around a vertical tube, Chun *et al.* [9] proposed an efficient method to predict the thickness of the solidified layer from the measured temperature of the tube wall.

Unlike normal fluids, pure water exhibits an eccen-

† Author to whom correspondence should be addressed.

NOMENCLATURE

c_r specific heat ratio, c_S/c_L
h_{sf} latent heat [J kg^{-1}]
$h_L(h_S)$ liquid (solid) phase enthalpy [J kg^{-1}]
H_0 initial height of water [m]
k_r thermal conductivity ratio, k_S/k_L
l length scale, $x_o - x_i$ [m]
m_S mass of ice formed [kg]
m_0 initial mass of water [kg]
$\overline{Nu}_w$ average Nusselt number
Pr Prandtl number
Ra Rayleigh number
Ste Stefan number
t time [s]
T temperature [°C]
T_0 initial temperature of water [°C]
T_f freezing temperature of water [°C]
T_i inner-tube-wall temperature [°C]
T_m density extremum temperature (~4°C)
ΔT temperature scale, $T_f - T_i$ [°C]
$V_L(V_S)$ volume occupied by the liquid (solid) phase [m^3]
x (y) radial (axial) coordinate [m]
x_i (x_o) radius of inner (outer) tube [m]
x_f interface position [m].

Greek symbols
$\delta_L(\delta_S)$ thickness of liquid (solid) phase [m]
η, ξ dimensionless transformed coordinates
θ_b dimensionless liquid bulk temperature
$\theta_L(\theta_S)$ dimensionless liquid (solid) enthalpy
θ_m equal to $(T_m - T_f)/\Delta T$
ν kinematic viscosity of water [m^2 s^{-1}]
ρ_r density ratio, ρ_S/ρ_L
τ dimensionless time, $\alpha_L t/l^2$.

Superscripts
0 old time t^0
+ dimensionless
− average.

Subscripts
0 initial
a average
L liquid
S solid.

tric behavior, namely, the nonlinear variation of its density with temperature. The effect of this density anomaly on natural convection has been of special interest [10–12]. (More recent works are well documented in ref. [12].) Here, emphasis is placed on the influence of the density anomaly upon phase-change via natural convection. A number of investigations have been carried out on this issue for various system configurations. Saitoh [13] shows that the Nusselt number has a local minimum when the flow direction reverses due to the density inversion. Saitoh and Hirose [14] consider freezing of water around a cooled horizontal tube and investigate numerically the overall effect of natural convection. The melting process of ice inside a horizontal cylinder is studied by Rieger and Beer [15]. Ho and Chen [16] consider outward melting of ice around a horizontal isothermal cylinder. Their numerical results predict the minimum average heat transfer to occur at a temperature different than that found experimentally by Herrmann *et al.* [17].

During phase transition, density difference between the solid and liquid phases causes the suction or blowing effect at the interface depending on which phase is at a greater density. Although the density difference has been commonly neglected in the literature, its effect increasingly called the attentions of researchers. Ho and Viskanta [18] discuss that the initial fluid flow during melting within a rectangular enclosure is due to the density difference accompanied with phase change. Similarly, an experimental study on melting inside a vertical tube [19] reveals that fluid flow is initially due to the volume expansion upon melting but, at later stages, is primarily due to natural convection. Prusa and Yao [20] include the effect of density difference in their analysis on melting around a heated horizontal cylinder, and find that temperature field and heat transfer rate are not affected significantly by the presence of density difference while the fluid flow is a little disturbed. Yoo and Ro [21] present a numerical simulation of melting within a rectangular enclosure considering density change. They find that better agreement with available experimental data is achieved by including the effect of density change. In light of these increased interests, the present analysis is tailored to account for the effect of density change for a quantitative investigation.

ANALYSIS

Problem description and physical model

A schematic of the physical model for the ice–water system considered in this study is depicted in Fig. 1. As shown there, a containment vessel composed of two concentric tubes is placed vertically, and water is partially filled within the enclosure up to an initial height H_0. An air gap is reserved on the top part of the enclosure to allow for volume expansion. The water is initially at a uniform temperature T_0 above its freezing temperature $T_f = 0$°C. The top and bottom sides of the containment vessel as well as its outer tube wall are kept thermally insulated. At time $t = 0$, the outside temperature of the inner tube wall is suddenly

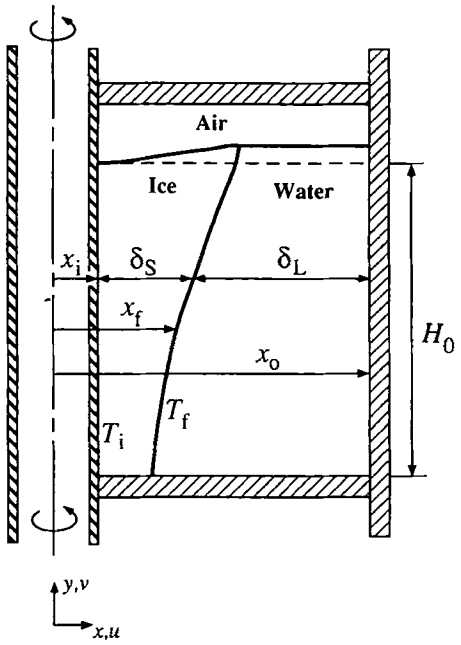

FIG. 1. Schematic diagram describing freezing of pure water in an axisymmetric enclosure.

lowered to a fixed value of $T_i < T_f$. Then, it is idealized that freezing occurs instantaneously at the outside of the inner tube and that an ice front, which is axisymmetrical and curved smoothly, propagates outward. The analysis further idealizes that fluid flow in the liquid is two-dimensional, Newtonian and laminar.

Basically, the freezing process under study goes through three stages with the passage of time. In an early stage of freezing, conduction is the prevailing mode of heat transfer and the ice front moves nearly parallel to the tube. After this conduction stage, natural convection becomes intense enough so that convective heat transfer takes over conduction. At this stage, a two-dimensional freezing pattern emerges owing to the nonuniform heat transfer rate at the interface. At a certain time, convective motion in the liquid reaches its highest vigor and then starts to calm down because of the reduction in the driving buoyancy force. The buoyancy reduction is of course attributable to a gradual decrease in the liquid bulk temperature. At a final stage of freezing, the liquid superheat diminishes substantially and, therefore, conduction again plays a primary role of heat transfer mechanism. These multiple stages of freezing are, irrespective of the material used, characteristic of solidification occurring in a bounded domain subject to the thermal boundary conditions as specified here, i.e. the isolated type mentioned earlier.

In addition, freezing with pure water being phase-change medium advances in a much more complicated fashion due to the well-known density inversion behavior in the vicinity of freezing temperature. To take this density anomaly of pure water into consideration, an available temperature–density correlation (in a range of 0–20°C) [22] is employed here as in other work [16]

$$\rho_L = \rho_m[1-\beta_T|T_L-T_m|^q] \tag{1}$$

where

$$\rho_m = 999.9720\,\mathrm{kg\,m^{-3}},\quad \beta_T = 9.297173\times10^{-6}\,^{\circ}\mathrm{C}^{-q}$$

$$T_m = 4.029325^{\circ}\mathrm{C},\quad q = 1.894816.$$

The above correlation is used only in determining the buoyancy force per unit volume (the Boussinesq approximation), i.e.

$$g\Delta\rho = g\beta_T\rho_m|T_L-T_m|^q \tag{2}$$

and thermodynamic and hydrostatic pressures are combined such that $p = p_{th}+\rho_m g y$. Otherwise, the thermophysical properties of water are assumed to be constant and their representative values are evaluated at an average (or film) temperature $T_a = (T_0+T_f)/2$.

When compared to common substances, water undergoes the largest density variation during liquid–solid phase transition (at 0°C, $\rho_L = 999.84\ \mathrm{kg\,m^{-3}}$ from equation (1) and $\rho_S = 917\ \mathrm{kg\,m^{-3}}$). This implies that the conventional assumption of negligible difference between ice and water densities may not be suitable to analyze the present problem. In this work, unequal densities are incorporated into the analysis in two ways; one is accounting for the non-zero velocity of liquid normal to the interface (from the interfacial mass balance) and the other no overflow of liquid on the top solid surface. The latter is based on the preliminary experimental observation [23]. A numerical implementation of density change into the present formulation is discussed in depth in the following section.

The major task to be undertaken is then the numerical integration of conservation equations over the solid and liquid domains whose shape and size vary with time. First, we write the general conservation equation with respect to the axisymmetric coordinate system in the following form

$$\frac{\partial}{\partial t}(x\rho\phi)+\frac{\partial}{\partial x}\left(x\rho u\phi-x\Gamma\frac{\partial\phi}{\partial x}\right)+\frac{\partial}{\partial y}\left(x\rho v\phi-x\Gamma\frac{\partial\phi}{\partial y}\right)=xS(x,y). \tag{3}$$

To circumvent the computational difficulties associated with directly working with the time-dependent domains of irregular shape, an algebraic coordinate transformation is employed

$$x=\begin{cases}x_i+\delta_S\xi, & 0\leqslant\xi\leqslant1\\ x_f+\delta_L(\xi-1), & 1\leqslant\xi\leqslant2\end{cases}$$

$$y = H\eta,\quad 0\leqslant\eta\leqslant1 \tag{4}$$

where $\delta_S = x_f-x_i$ and $\delta_L = x_o-x_f$. Then, in the transformed coordinate the interface is immobilized at $\xi = 1$, and the top ice and water surfaces are immobilized at $\eta = 1$ at all times. It is assumed here that

$H = H(\xi, t)$ for the solid phase and $H = H(t)$ for the liquid phase. In accord with the introduction of the new coordinate system, the general conservation equation is also transformed and a complete list of the transformed equations is given elsewhere [24].

The boundary conditions are specified except at the interface

$$\begin{aligned} T &= T_i && \text{at } \xi = 0 \\ \partial T/\partial x = 0, \quad u = v &= 0 && \text{at } \xi = 2 \\ \partial T/\partial y = 0, \quad u = v &= 0 && \text{at } \eta = 0 \\ \partial T/\partial y = \partial u/\partial y &= 0, \quad v = \mathrm{d}H/\mathrm{d}t && \text{at } \eta = 1 \end{aligned} \quad (5)$$

all of which should be appropriately transformed prior to discretization. The interfacial conditions are basically the same as those elaborated in ref. [24] except density change. For the energy equation, enthalpy is chosen as the dependent variable and is defined in each phase as

$$h_S = c_S(T_S - T_f) - h_{sf}, \quad h_L = c_L(T_L - T_f). \quad (6)$$

To simplify the analysis, dimensionless groups are introduced such that

$$\tau = \frac{\alpha_L t}{l^2}, \quad \rho^+ = \frac{\rho}{\rho_a}, \quad x^+ = \frac{x}{l}, \quad y^+ = \frac{y}{l}$$

$$\theta_S = \frac{h_S}{c_L \Delta T}, \quad \theta_L = \frac{h_L}{c_L \Delta T}, \quad u^+ = \frac{ul}{\alpha_L}$$

$$v^+ = \frac{vl}{\alpha_L}, \quad p^+ = \frac{pl^2}{\rho_a \alpha_L^2}, \quad Pr = \frac{\nu}{\alpha_L}$$

$$Ra = \frac{\rho_m}{\rho_a} \frac{g\beta_T(\Delta T)^q l^3}{\alpha_L \nu}, \quad Ste = \frac{c_L \Delta T}{h_{sf}}. \quad (7)$$

Accordingly, the dimensionless conservation equations used in the analysis are obtained and summarized in Table 1.

Solution procedure

A finite control-volume approach [25] was employed to discretize the transformed conservation equations. To account for the axisymmetric geometry, a numerical method recently developed by Kim *et al.* [24], which is a general extension of the method suggested in ref. [26], was adopted for its superior performance in handling multiple moving boundaries and density difference between phases. A fundamental benefit of their method is that the conservation quantities are faithfully preserved. In their work, the time-dependent volume elements and the combined pseudo-velocities are discretized according to the extended area rule that is self-satisfactory from the geometrical point of view. This elaborately designed procedure unveiled that the factor x due to the axisymmetric geometry should be *dually* evaluated to preserve global mass conservation.

Table 1. Variables in the dimensionless governing equations

	ρ^+	ϕ^+	Γ^+	S^+
Solid	ρ_r	1	0	0
		θ_S	k_r/c_r	0
Liquid	1	1	0	0
		u^+	Pr	$-\partial p^+/\partial x^+ - Pr \cdot u^+/x^{+2}$
		v^+	Pr	$-\partial p^+/\partial y^+ + Ra \cdot Pr\,\lvert\theta_L - \theta_m\rvert^q$
		θ_L	1	0

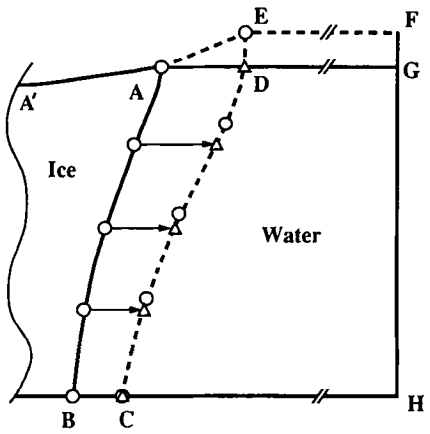

FIG. 2. Illustration of manipulating density change. Lines ADG and EF are horizontal, and lines DE and GF are vertical.

A nonuniform grid system is used by deploying 23 nodes in the radial direction and 31 nodes in the axial direction. Such an arrangement was chosen after considering that the grid system of similar resolution [26] successfully simulated existing experimental results [5]. For the start-up of computation, an ice layer of thickness $\delta_S/x_i = 0.01$ is assumed to exist initially. The interface movement is controlled by using a variable time step such that the maximum changes in both δ_S and δ_L remain within 1%.

Figure 2 illustrates schematically how to manipulate volume expansion upon freezing. It is assumed that the height of the free surface is a function of time only. Suppose that the domain boundaries of the solid and liquid phases are all known at the old time t^0. In Fig. 2, AB designates the interface; AA′ the ice top surface; and ADG the free surface at time t^0, respectively. Since the ice remains motionless during solidification, only a part of it is shown in the Figure. The interface is approximated by a cluster of points marked by circles but only a few points are drawn to aid visual clarity. With the known temperature distribution in each phase, the interfacial mass flux can be found from the conservation of heat flux across the interface (details are given in ref. [24]). Then, a tentative interface position is obtained by translating the circles in a horizontal direction and falling onto the triangles, as shown in the Figure. To consider the density difference between ice and water, an overall mass balance is utilized to explicitly determine the new height of the free surface

$$(\rho_L - \rho_S)\tilde{m}(\mathrm{ABCD}) = \rho_S \tilde{m}(\mathrm{ADE}) + \rho_L \tilde{m}(\mathrm{DEFG}) \quad (8)$$

where $\tilde{m}$(ABCD) denotes the positive value of the volume enclosed by ABCD, and so forth. Finally, the interface position at the new time $t^0+\Delta t$ is determined by proper interpolation of the tentative interface, as indicated by the circles on the dotted line in Fig. 2. Then, AE designates the newly-formed ice surface and EF represents the free surface at time $t^0+\Delta t$. Similarly, the ice top surface is also redistributed by interpolation. This procedure was preferred due to its simplicity, and it was justified from the fact that an overall mass balance (i.e. the condition $m_0 = \rho_S V_S + \rho_L V_L$) was satisfied to within 0.0001% at each time step. Also, an overall energy balance was checked at each time step and found to be satisfied to within a tolerance of 0.1%.

RESULTS AND DISCUSSION

Numerical simulation of freezing of water filled within vertical concentric tubes was carried out for two inner-tube-wall temperatures, $T_i = -10, -20°C$, and three initial superheats of water, $T_0 = 4, 10, 15°C$ ($Pr = 13.55$; $Ra = 3.03\times10^7$ and $Ste = 0.131$ for $T_i = -10°C$; $Ra = 1.13\times10^8$ and $Ste = 0.262$ for $T_i = -20°C$). The system configuration was fixed with $x_i = 1$ cm, $x_o = 11$ cm and $H_0 = 20$ cm. Together with the numerical solution to the present formulation, one-dimensional pure conduction solution was obtained for comparison by neglecting the convective motion due to the buoyancy and density change.

Before we discuss our numerical results, we hope to mention several basic features specific to the present problem. In this regard, Fig. 3 is prepared in which pure conduction solution is drawn schematically. In the absence of convection the interface and isotherms advance perfectly parallel to the tube wall, as shown in the upper panel. For brevity, the case $T_0 > T_m$ is considered in the Figure, and the freezing and density-inversion isotherms (i.e. T_f and T_m) are highlighted

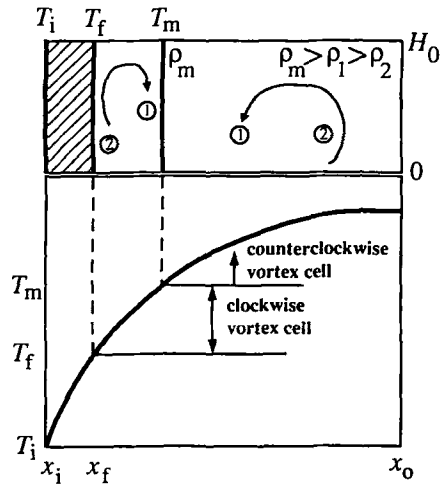

FIG. 3. Pure conduction solution at a certain time. The drawing is not to scale.

due to their significance (the latter isotherm does not exist when $T_0 < T_m$). In the lower panel, the underlying assumption of the continuity of temperature is clearly stated. Now, suppose that natural convection is promptly taken into consideration from this point on. It is then likely that at least qualitative trends can be inferred from the Figure. Firstly, in the case of $T_0 < T_m$ only a single vortex circulating clockwise develops in the liquid. Secondly, when $T_0 > T_m$, double vortices would develop on both sides of the T_m-isotherm with their flow directions opposite to each other, as shown in the Figure. For the Prandtl number of unity, the T_m-isotherm would closely coincide with the boundary separating the two vortices. Noting that the counterclockwise circulation is sponsored by the liquid superheat over the temperature T_m, we anticipate that it will eventually die out with disappearance of the T_m-isotherm. Meanwhile, the clockwise circulation enjoys longevity until the water is completely saturated. This implies that coexistence of double vortices takes place for a limited duration of time even when $T_0 > T_m$.

Figure 4 provides sequential contour plots to expose the timewise progression of fluid flow and temperature distribution in the liquid for the case of $T_0 = 4°C$ and $T_i = -20°C$. Stream function is defined as in ref. [24], and the isotherms are drawn by an equal increment $0.1(T_0 - T_f)$. An early stage of freezing can be easily recognized from Fig. 4(a) in which the isotherms are nearly parallel to the vertical over most of the height indicating the predominance of heat conduction. As the water close to the interface cools down, its density attains a value lower than that of the water far from the interface. Accordingly, the relatively lighter water moves upward along the interface, and near the top changes its flow direction toward the outer tube wall. This fluid motion disturbs temperature distribution in the vicinity of the top interface such that isotherms are impelled to spread outward and, as a result, freezing is locally enhanced. On the other hand, the relatively heavier water (thus at higher temperature) impinges on the bottom interface, thereby retarding the rate of freezing due to the higher temperature gradient induced there. However, an augmented freezing near the top interface encounters, by virtue of the axisymmetric geometry, a more enlarged area than the average, while an impeded freezing near the bottom interface encounters a more contracted area. Therefore, the axial variation of the frozen layer thickness tends to be quite moderate, as opposed to the case of planar freezing [8]. Figure 4(a) also shows that, since momentum diffuses faster ($Pr > 1$), an upflow region spans a wider distance than the thermal propagation layer. In the upper panels of Figs. 4(b)–(e), a succeeding deformation pattern of isotherms is portrayed (isotherm plots are omitted when the maximum temperature in the liquid is below 10% of the initial superheat). Because the gravity force exerts to stabilize the thermal field, isotherms are stratified outside the thermal boundary layer, as indicated by a

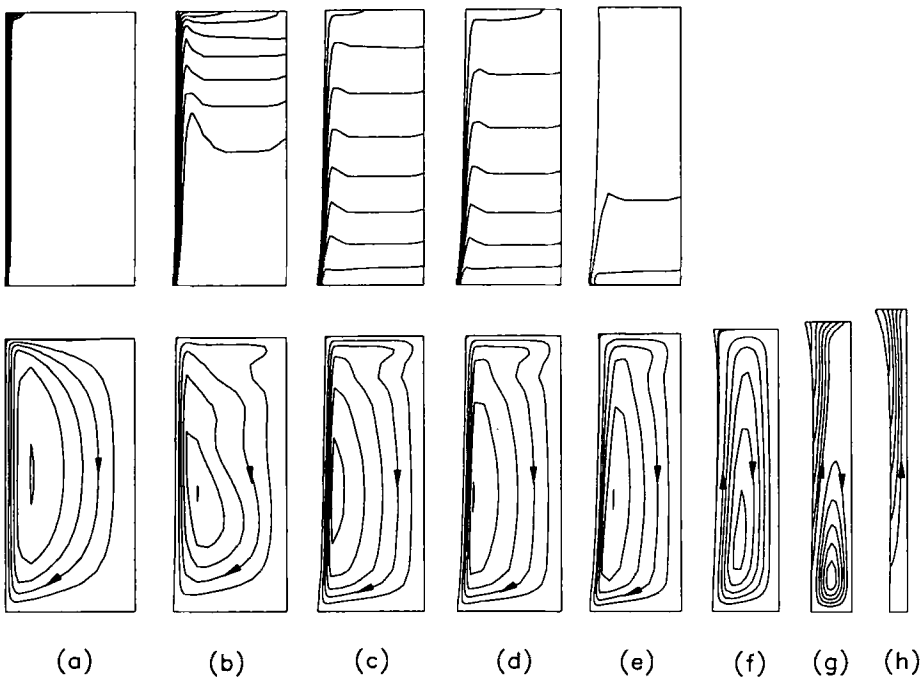

FIG. 4. Sequential contour plots for isotherms (upper panels) and streamlines (lower panels) for $T_i = -20°C$ and $T_0 = 4°C$. The dimensionless time τ is (a) 0.00074, (b) 0.0238, (c) 0.0634, (d) 0.0738, (e) 0.1476, (f) 0.2952, (g) 0.5167 and (h) 0.8119. A real time of 30 min corresponds to $\tau = 0.0238$.

stack of plateaus. An event worthy of special remark is spotted in Fig. 4(g) that reveals what the flow pattern looks like at the final stage of freezing. As is shown there, a weak vortex with its center located far below persists owing to the regional survival of a small amount of superheat. Moreover, a bunch of streamlines are launched at the interface and travel toward the top free surface. This ascending fluid motion is caused not by buoyancy but by the incompressibility and density difference. Actually, it has been in the proximity of the interface from the beginning, and only at the final stage of freezing does it attain such a vitality as comparable to the vortex strength. Later as the liquid becomes completely saturated (Fig. 4(h)), there exists the ascending fluid motion only.

Figure 5 exhibits how the flow pattern and isotherm distribution evolve with time when the initial superheat is above the maximum density point. The results shown there are representative of freezing with $T_0 > T_m$. In Fig. 5(a), which pertains to a small elapsed time, the freezing and density-inversion isotherms enclose so extremely narrow a region that the intensity of clockwise vortex is negligibly weak (see Fig. 3). Consequently, developed in the liquid is a single vortex cell the direction of which is reversed compared to the case of lower superheat ($T_0 < T_m$). The isotherms are mostly parallel to the vertical as well, but their lower parts stretch outward in accord with the flow reversal. Figure 5(b) shows that a clockwise vortex of small size is newly formed near the bottom interface. This clockwise vortex cell begins to mature along the interface (Fig. 5(c)). Subsequently, it competes with (Figs. 5(d)–(e)) and then overwhelms its counterpart (Figs. 5(f)–(g)). It is also noted that the density-inversion isotherm (the fifth one in the Figure, counting the interface as the first) approximately separates two competing cells, as expected. The timewise deformation of isotherms occurs not so monotonic as in Fig. 4, but in an apparently whimsical manner. Especially, the isotherm patterns shown in Figs. 5(b) and (f) are flipped vertically in consistence with transposing of the dominant vortex cells. The final stage of freezing (Figs. 5(h)–(i)) resembles that shown in Fig. 4, because the liquid becomes nearly or completely saturated and thus the initial superheat is no longer a meaningful parameter.

Figures 6 and 7 display the transient positions of the interface at several prescribed times for all the cases considered. The thicker lines denote the inner tube wall as well as the top surface of the ice. Numerical results show that the ice top surface is noticeably curved upward. Since the interface movement subject to the temperature change at the inner tube wall proceeds in an analogous manner, attention is turned to the results shown in Fig. 6.

In the case of lower superheat (Fig. 6(a)), the interfaces appear plainly curved with mild curvatures. As the clockwise vortex develops in the liquid, freezing is expedited/hindered in the upper/lower portion. Therefore, the interfaces become slanted with positive slopes. As convective motion ceases later, the interface movement is primarily controlled by heat conduction,

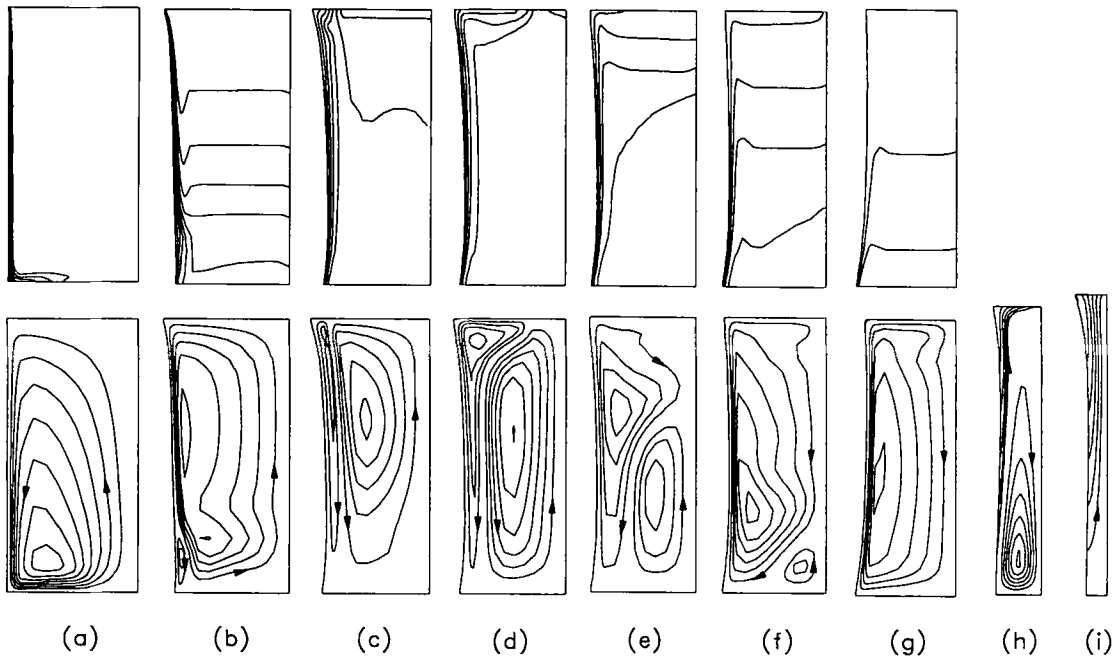

FIG. 5. Isotherms (upper panels) and streamlines (lower panels) for $T_i = -20°C$ and $T_0 = 10°C$. The dimensionless time τ is (a) 0.00074, (b) 0.0238, (c) 0.0634, (d) 0.0738, (e) 0.0886, (f) 0.1033, (g) 0.1476, (h) 0.5176 and (i) 0.8119.

thereby driving the frozen layer thickness to be more uniform. Interestingly, it can be seen that the interface movement lags near the top enclosure at the final stage of freezing. This is due to the fact that heat conduction in the solid is apt to trek as long a distance in the top as it does in the bottom.

In response to the growth history of the clockwise vortex cell, freezing with higher superheat gives rise to a complex marching pattern of the interface, as shown in Figs. 6(b)–(c). Initially, the frozen layer grows with its thickness largest in the bottom (owing to the presence of a single counter-clockwise vortex). As a small clockwise vortex cell develops near the bottom interface, freezing is *locally* retarded/enhanced at the foot/head of the small cell. Still, the predominant counter-clockwise vortex hinders the growth of frozen layer near the top interface (see Fig. 5(b)). Then, the combined effect of double cells is to make the interface bulge outward by holding its two ends. As freezing continues further, protrusion of the interface into the liquid proceeds markedly ($\tau = 0.0634$). This phenomenon was also confirmed experimentally in ref. [23]. Until the clockwise vortex cell rises along the interface up to the free surface, the

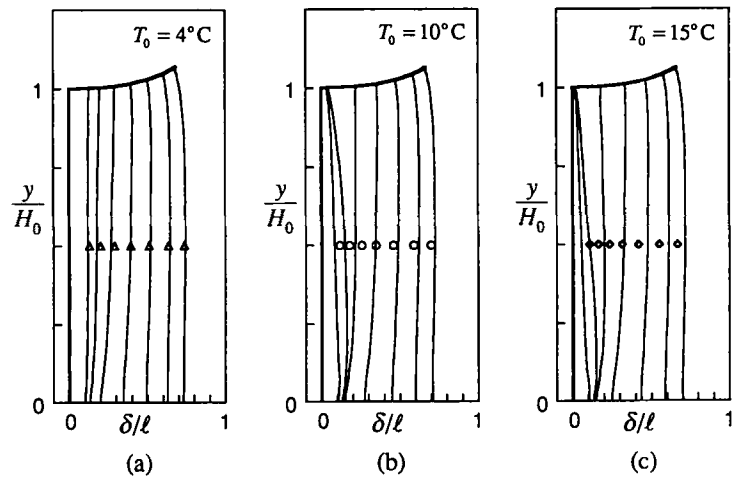

FIG. 6. The predicted results for the interface locations at $\tau = 0.0238, 0.0634, 0.1476, 0.2952, 0.5167, 0.8119, 1.1072$ (left to right) for $T_i = -10°C$.

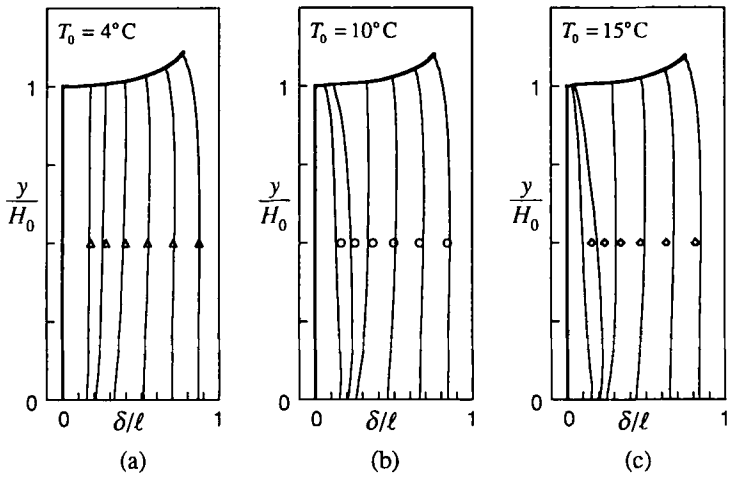

FIG. 7. The predicted interface locations at $\tau = 0.0238, 0.0634, 0.1476, 0.2952, 0.5167, 0.8119$ (left to right) for $T_i = -20°C$.

top edge of the interface remains anchored for a while indicating that heat fluxes are almost balanced there. After the T_m-isotherm fades away, the interface marches in a way similar to the previous case of lower superheat.

Additionally, comparison with pure conduction solutions (symbols in the Figure) clearly reveals an overall role played by natural convection. Earlier, natural convection is contributory to global mixing of the thermal field and delivering more energy to the interface. Therefore, freezing is impeded as indicated by the interface lagging behind the symbols. With further freezing, the liquid becomes less superheated since more energy has been extracted from it and hence the average interface location catches up with that of the pure conduction solution. The liquid gets saturated sooner than the case of pure conduction, and freezing is, on an average, expedited. In this matter, Figs. 6 and 7 dictate that the higher the liquid superheat, the stronger the *overall* effect of natural convection. This reasoning is also manifested in Fig. 8 where the frozen mass fraction is plotted with respect to the dimensionless time. It can be seen that deviation from the pure conduction solutions magnifies with an increase in the liquid superheat. Also reaffirmed in the Figure is that freezing is initially retarded but is expedited finally (as demonstrated by the relative location of symbols to curves). In general, the ice mass fraction varies linearly with time except for the small times. A simple order-of-magnitude analysis would be helpful to explain this behavior. Let us assume that an average thickness of the ice layer is approximately $\delta_S \sim \sqrt{t}$ with its proportionality factor being a moderately varying function of time. Such a notion is obviously borrowed from the well-known Stefan solution for the semi-infinite plane problem where the numerical value of $\delta_S/\sqrt{t}$ remains constant. Since the frozen mass is approximately of the order

$$m_S \sim \delta_S(\delta_S/2 + x_i) \tag{9}$$

we have $m_S \sim \sqrt{t}$ when $\delta_S \ll x_i$. At larger times (or when $\delta_S \gtrsim x_i$), we deduce that $m_S \sim t$ by taking the leading term only. Although this analysis is not very rigorous, it is possible to qualitatively validate the results shown in Fig. 8.

The variation of normalized bulk temperature of water, θ_b/θ_0, vs the dimensionless time is shown in Fig. 9. The dimensionless bulk temperature of water was defined as

$$\theta_b = \frac{\int_{V_L} \rho_L \theta_L \, dV}{\int_{V_L} \rho_L \, dV} \tag{10}$$

the value of which is evaluated by the numerical integration. As expected, θ_b decreases at a rate faster than the case of pure conduction. It is interesting that θ_b vanishes at $\tau \sim 0.4$ for $T_i = -10°C$, and at $\tau \sim 0.3$ for $T_i = -20°C$, respectively, independent of T_0. This

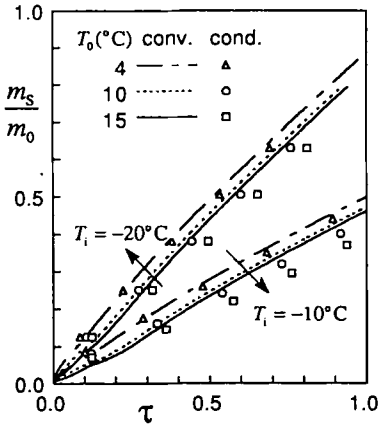

FIG. 8. Ice mass fraction vs dimensionless time. Symbols denote pure conduction solutions.

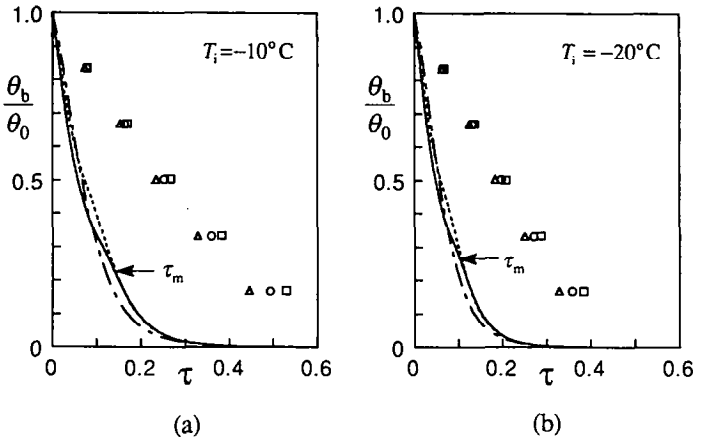

FIG. 9. Normalized liquid bulk temperature with respect to dimensionless time. (a) $T_i = -10°C$ and (b) $T_i = -20°C$. See Fig. 8 for legends.

decay time seems to be rather dependent on the system configuration and the value of T_i. Further inspection reveals that two curves corresponding to the cases of $T_0 > T_m$ merge together when $\tau > \tau_m$. The merging time τ_m indeed occurs when the density-inversion isotherm disappears (note that $\tau_m \sim 0.1$ in Fig. 9(b) and $\tau = 0.1033$ in Fig. 5(f)). It is also noted that for a certain duration of time below τ_m the rate of decrease in θ_b is weakened noticeably, and this temporal damping is definitely associated with the competing action of the double vortices. When $\tau > \tau_m$, θ_b decreases monotonously as in the case of $T_0 < T_m$.

The history of the heat transfer rate at the inner tube wall is depicted in Fig. 10. The average Nusselt number as defined in the Figure initially shows a rapid decrease due to the sudden jump condition at the tube wall, but its variation with time is substantially reduced later. The Nusselt numbers Nu_1 and Nu_2 represent the dimensionless heat transfer rates evaluated from the steady-state pure conduction solutions by locating the interface at the midpoint of the enclosure

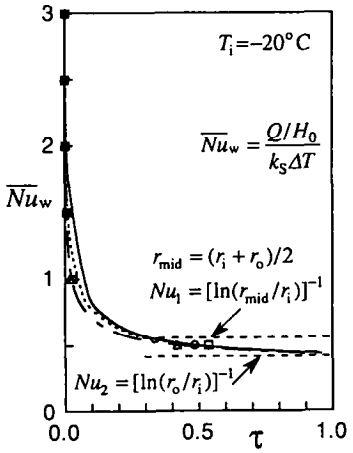

FIG. 10. Timewise variation of the dimensionless heat transfer rate $\overline{Nu}_w$ at the inner tube wall for the case of $T_i = -20°C$. See Fig. 8 for legends.

and at the outer tube wall, respectively. It can be seen that at larger times the variation of $\overline{Nu}_w$ coincides well with that of the pure conduction solution, as can be expected from the marching pattern of the interfaces shown in Fig. 7. While Fig. 8 shows a lesser amount of ice formed at small times (compared to the pure conduction case), the variation of $\overline{Nu}_w$ indicates that more energy is being extracted from the system; therefore, we conclude that a large proportion of the energy is used to extract the sensible heat of water in the presence of natural convection.

SUMMARY

Investigation on freezing of water was undertaken considering density anomaly and volume expansion. Numerical simulation of the present problem was successful in exemplifying the versatility of the numerical method developed by the authors. Two types of thermal boundary conditions were identified to distinguish whether natural convection in the liquid tends to be everlasting or evanescent. This clarification enabled us to recognize the general characteristics of the freezing process considered here. In accordance with the imposed thermal boundary conditions, as identified herein, of *isolated* type, the effect of natural convection was significant at early times but damped out later. Inclusion of volume expansion upon freezing clearly revealed that two-dimensional freezing is inevitable even in the absence of natural convection. In general, the freezing proceeds undergoing three stages with time, i.e. the initial conduction-controlled stage followed by the convection-dominant one, and the final conduction-controlled stage again. Especially when the liquid is superheated above the density-extremum temperature, the transient and local characteristics of fluid flow and temperature distribution are markedly changing with time and thus freezing pattern is more complicated. An accepted fact that natural convection retards the movement of the inter-

face was also confirmed here. However, it should be noted that solidification itself is ultimately expedited because the liquid bulk temperature drops faster owing to the mixing-up by natural convection.

Acknowledgement—This research was carried out under the financial support of the Korea Science and Engineering Foundation (KOSEF) through the Seoul National University, for which the authors are grateful.

REFERENCES

1. R. Viskanta, Phase-change heat transfer. In *Solar Heat and Storage: Latent Heat Materials* (Edited by G. A. Lane), Vol. 1, pp. 153–222. CRC Press, Boca Raton, Florida (1983).
2. R. Viskanta, Natural convection in melting and solidification. In *Natural Convection: Fundamentals and Applications* (Edited by S. Kakac *et al.*), pp. 845–877, Hemisphere, Washington, D.C. (1985).
3. L. S. Yao and J. Prusa, Melting and freezing, *Adv. Heat Transfer* **19**, 1–95 (1989).
4. E. M. Sparrow, J. W. Ramsey and R. G. Kemink, Freezing controlled by natural convection, *J. Heat Transfer* **101**, 578–584 (1979).
5. C. Benard, D. Gobin and A. Zanoli, Moving boundary problem: heat conduction in the solid phase of a phase-change material during melting driven by natural convection in the liquid, *Int. J. Heat Mass Transfer* **29**, 1669–1681 (1986).
6. C.-J. Ho and R. Viskanta, Heat transfer during inward melting in a horizontal tube, *Int. J. Heat Mass Transfer* **27**, 705–716 (1984).
7. A. Gadgil and D. Gobin, Analysis of two-dimensional melting in rectangular enclosures in presence of convection, *J. Heat Transfer* **106**, 20–26 (1984).
8. N. Ramachandran, J. P. Gupta and Y. Jaluria, Two-dimensional solidification with natural convection in the melt and convective and radiative boundary conditions, *Numer. Heat Transfer* **4**, 469–484 (1981).
9. M.-H. Chun, H.-O. Choi, H.-G. Jun and Y.-S. Kim, Phase-change front prediction by measuring the wall temperature on which solidification occurs, *Int. J. Heat Mass Transfer* **30**, 2641–2650 (1987).
10. H. J. Merk, The influence of melting and anomalous expansion on the thermal convection in laminar boundary layer, *Appl. Sci. Res.* **4**, 435–452 (1953).
11. C. R. Vanier and C. Tien, Further work on free convection in water at 4°C, *Chem. Engng Sci.* **22**, 1747–1751 (1967).
12. S. L. Braga and R. Viskanta, Transient natural convection of water near its density extremum in a rectangular cavity, *Int. J. Heat Mass Transfer* **35**, 861–875 (1992).
13. T. Saitoh, Natural convection heat transfer from a horizontal ice cylinder, *Appl. Sci. Res.* **32**, 429–521 (1976).
14. T. Saitoh and K. Hirose, Numerical method for the two-dimensional freezing problem around a horizontal cylinder encompassing a density inversion point, *Bull. JSME* **24**, 147–152 (1981).
15. H. Rieger and H. Beer, The melting process of ice inside a horizontal cylinder: effects of density anomaly, *J. Heat Transfer* **108**, 166–173 (1986).
16. C. J. Ho and S. Chen, Numerical simulation of melting of ice around a horizontal cylinder, *Int. J. Heat Mass Transfer* **29**, 1359–1369 (1986).
17. J. Herrmann, W. Leindenfrost and R. Viskanta, Melting of ice around a horizontal isothermal cylindrical heat source, *Chem. Engng Commun.* **25**, 63–78 (1984).
18. C.-J. Ho and R. Viskanta, Experimental study of melting in a rectangular cavity. In *Heat Transfer*—1982 (Edited by U. Grigull *et al.*), Vol. 2, pp. 369–374. Hemisphere, Washington, D.C. (1982).
19. E. M. Sparrow and J. A. Broadbent, Inward melting in a vertical tube which allows free expansion of the phase-change medium, *J. Heat Transfer* **104**, 309–315 (1982).
20. J. Prusa and L. S. Yao, Effect of density change and subcooling on the melting of a solid around a horizontal heated cylinder, *ASME* paper No. 84-HT-3 (1984).
21. H. Yoo and S. T. Ro, Melting process with solid–liquid density change and natural convection in a rectangular cavity, *Int. J. Heat Fluid Flow* **12**, 365–374 (1991).
22. B. Gebhart and J. Mollendorf, A new density relation for pure and saline water, *Deep Sea Res.* **24**, 831–848 (1977).
23. M. G. Kim, Study on ice storage process around a vertical tube considering solid–liquid density change and natural convection, Ph.D. Thesis (in Korean), Seoul National University, Seoul, Korea (1991).
24. C.-J. Kim, S. T. Ro and J. S. Lee, An efficient computational technique to solve the moving boundary problems in the axisymmetric geometry, *Int. J. Heat Mass Transfer* (in press).
25. S. V. Patankar, *Numerical Heat Transfer and Fluid Flow*, Hemisphere, Washington, D.C. (1980).
26. C.-J. Kim and M. Kaviany, A numerical method for phase-change problems with convection and diffusion, *Int. J. Heat Mass Transfer* **35**, 457–467 (1992).